

ehp

**ENVIRONMENTAL
HEALTH
PERSPECTIVES**

ehponline.org

**Heavy Metal Lead Exposure, Osteoporotic-like
Phenotype in an Animal Model,
and Depression of Wnt Signaling**

**Eric E Beier, Jason R Maher, Tzong-Jen Sheu,
Deborah A Cory-Slechta, Andrew J Berger,
Michael J Zuscik, Edward J Puzas**

<http://dx.doi.org/10.1289/ehp.1205374>

Online 19 October 2012



NIEHS

**National Institute of
Environmental Health Sciences**

**National Institutes of Health
U.S. Department of Health and Human Services**

Heavy Metal Lead Exposure, Osteoporotic-like Phenotype in an Animal Model, and Depression of Wnt Signaling

Authors

Eric E Beier ^{1,2}, Jason R Maher ³, Tzong-Jen Sheu ¹, Deborah A Cory-Slechta ², Andrew J Berger ³, Michael J Zuscik ¹, Edward J Puzas ^{1,2}

¹Center for Musculoskeletal Research, ²Department of Environmental Medicine, University of Rochester, School of Medicine and Dentistry, Rochester, New York, USA; and ³The Institute of Optics, University of Rochester, Rochester, New York, USA.

Corresponding author

J. Edward Puzas, Ph.D.

601 Elmwood Avenue

Rochester, New York 14642

Phone: (585) 275-3664, Fax: (585) 756-4727

Email: Edward_puzas@urmc.rochester.edu

Acknowledgements

We thank R Tierney and S Mack for assistance with histology, R Gelein for bone Pb measurements, M Thullen for CT imaging and analysis, E Resseguie for gathering adipocyte metrics, and C Muzytchuk for DXA measurements. Biomechanical testing was performed with assistance from Drs. H Awad and T Chen in the Biomechanics and Multimodal Tissue Imaging Core laboratory, established by NIH grant # P30AR061307. This work was supported by Public Health Service grants: NIH T32 ES07026 and R01 ES012712, T32 AR053459, P01 ES011854, and P30 ES301247.

Short Title

Pb induces an osteoporotic-like phenotype

Key Words

Bone mineral density, lead, mesenchymal stem cells, rat, Wnt signaling

None of the authors has any actual or potential competing financial interests.

Abbreviations: Blood lead level (BLL), bone mineral density (BMD), carbonate-to-phosphate ratio (CTPR), dual-energy x-ray absorptiometry (DXA), and mineral-to-matrix ratio (MTMR).

Abstract

BACKGROUND: Exposure to lead from environmental and industrial sources remains an overlooked serious public health risk. Elucidating the effect of lead on bone cell function is therefore critical for understanding its risk associated with diseases of low bone mass.

OBJECTIVES: We tested the hypothesis that lead negatively effects bone mass and assessed the underlying mechanisms of lead on bone signaling pathways.

METHODS: We used a model of low-level lead exposure in a rodent beginning before conception and continuing over 18 months. We characterized the effect of Pb on bone quality using DXA, micro-CT, Raman spectroscopy, and histology. We assessed the effect of lead on bone and adipocyte formation by mineral deposition, lipid droplet formation, and Western and RNA analysis.

RESULTS: Lead-exposed animals had decreased bone mass that resulted in bones that were more susceptible to fracture. Lead decreased osteoblastic cell number leading to a depression of bone formation. Accompanying this, lead exposure elevated sclerostin protein levels in the skeleton, and correspondingly reduced levels of β -catenin and Runx2 in stromal precursor cells. Lead also increased skeletal *PPAR- γ* expression. These results indicate a shift in mesenchymal differentiation wherein lead promoted enhanced adipogenesis and decreased osteoblastogenesis. Substantial differences in bone marrow composition were observed, highlighted by an increase in adipocytes.

CONCLUSIONS: The disruption of lead on bone mass and bone homeostasis is principally explained by inhibition of the Wnt/ β -catenin pathway which may provide a molecular basis for novel therapeutic strategies to combat lead induced bone pathologies.

Introduction

Although attempts have been made to decrease the amount of lead (Pb) in the environment, it remains a pervasive toxicant contributing to problems for human health. In the 1970s greater than 75% of Americans had blood lead levels (BLL) above 10 $\mu\text{g}/\text{dL}$ (Mahaffey et al. 1982), which is where the current adopted threshold of concern resides as defined by the Centers for Disease Control (CDC 1991). Although the average BLL has declined, developmental and lifelong low Pb exposures are recognized as having a persistent negative impact on human health (Goyer 1993). These serious Pb-related health issues, notably in the skeleton, can occur below the current threshold BLL of concern.

Previously underappreciated, recent clinical and basic science research suggests that Pb has a profound influence on both the developing and adult skeleton. Reports in animals (Bagchi and Preuss 2005; Escribano et al. 1997; Gruber et al. 1997) and humans (Campbell and Auinger 2007; Nash et al. 2004) have begun to associate a detrimental impact of cumulative Pb burden on bone mineral density (BMD) and development of osteopenias. We have previously found an inverse correlation with rats exposed to increasing levels of Pb for 6 weeks in their drinking water and decreased total body BMD (Bagchi and Preuss 2005). In NHANES III (1988-1994), there was also a significant inverse correlation between blood lead levels and femoral BMD (Nash et al. 2004). Despite these observations, attempts at describing a mechanism of skeletal Pb toxicity remain elusive.

Osteoporosis is a progressive disease characterized by a reduction in BMD sufficient to reduce biomechanical strength and increase fracture risk. We postulate that subsequent weakening of skeletal structure due to decreased osteoblast activity by Pb increases the risk of osteoporosis. This is supported uniformly by numerous literature reports that Pb negatively

impacts osteoblast function *in vitro* (Dowd et al. 2001; Klein and Wiren 1993; Puzas et al. 2004; Sauk et al. 1993).

One key signaling pathway coordinating bone homeostasis is the Wnt/ β -catenin pathway. Activation of this pathway occurs with binding of Wnt agonists to the frizzled receptor that stabilizes β -catenin (unphosphorylated) in the cytoplasm as a result of a disassociation of the negatively regulating complex consisting of glycogen synthase kinase 3 β , Axin, Frat1, and Disheveled. There have been numerous efforts in recent years to delineate this pathway and understand the impact of bone-specific Wnt molecules. Several genetic models have illustrated the importance of β -catenin function on mesenchymal lineage specification (Shahnazari et al. 2008) and on bone homeostasis (Johnson et al. 2004; Robinson et al. 2006). These efforts led to the discovery of the Wnt antagonist, sclerostin (Johnson et al. 1997), which was shown to bind to LRP5 and LRP6 with high affinity, co-receptors that are required for transduction of canonical Wnt signals (Li et al. 2005). Sclerostin was further documented by several groups to be a very potent inhibitor of bone formation through its repression of osteoblast function (Li et al. 2008, Li et al. 2009; van Bezooijen 2005). Studies from our lab indicate a strong Pb induction of sclerostin that could provide new insights into a molecular mechanism of disruption of bone homeostasis by inhibition of Wnt signaling.

Our objective in this study is to evaluate bone quality in female rats exposed to physiologically low levels of Pb over a lifetime, mimicking a plausible human exposure. This report describes the observed phenotype with specific focus on clinical correlates of dual-energy x-ray absorptiometry (DXA) analysis, chemical composition using optical spectroscopy, and biomechanical strength testing, as well as exploring the modulation of Pb on Wnt signaling as the driving force for these effects.

Methods

Animals and Pb Exposure. We randomly split Long-Evans rats into two groups to receive water containing 0 or 50 ppm Pb acetate two months prior to breeding to obtain elevated Pb body burden at conception. Female offspring (9 rats/group) were continuously exposed to Pb for the duration of their life (Cory-Slechta et al. 2010). Blood Pb samples were provided by tail nicks and were analyzed by anodic stripping voltammetry using the Lead Care II system. We then anesthetized the animals and perfused them with either phosphate buffered saline or 10% formalin. We harvested skeletal elements and assessed phenotype. All animals were treated humanely and with regard for alleviation of suffering.

Bone Pb determination, RNA isolation and real time reverse transcription-polymerase chain reaction (RT-PCR). We isolated right tibiae, discarded the epiphyses and soft tissues, and flushed the bone marrow with a 25-gauge 5/8-inch needle (Becton-Dickinson, Franklin Lakes, NJ). We homogenized four bones/group and extracted RNA using TRI Reagent (MRC Inc., Cincinnati, OH) according to the manufacturer's recommendation followed by DNase digestion and column separation using QIAGEN mini columns. We then performed reverse transcription using the iScript cDNA synthesis kit from Bio-Rad (Hercules, CA), and carried out RT-PCR reactions using PerfeCTa SYBER green (Quanta, MD) according to manufacturer's protocols. Gene of interest was normalized with β -actin expression. For primer sequences see Supplemental Material, Table S1. For bone Pb, we washed four flushed diaphyseal bones/group with PBS and incubated in 3% hydrogen peroxide for 20 minutes. We then processed the bones as described previously (Carmouche et al. 2005; Parsons 1993) and analyzed the samples using atomic absorption spectroscopy.

Radiography, Bone densitometry and Micro-CT. We obtained radiographic images using a Faxitron cabinet X-ray system (Faxitron, Wheeling, IL) on 9 rats/group. The images were thresholded to remove soft tissue elements. We determined areal BMD from rats *ex vivo* by DXA (GE Lunar Advance). The region of interest (ROI) included the lumbar vertebrae (LV₁–LV₅) and femur-tibia.

We determined bone properties using a 10.5- μ m resolution micro-CT scanner as described previously (Guo et al. 2008) (Scanco Medical, Basserdorf, Switzerland). For trabecular bone analyses within the distal femur and proximal tibia, a region equivalent to 8% of the femur height (2.6 mm) was selected beginning 0.3 mm from the most proximal aspect of the growth plate scanned and images were reconstructed to an isotropic voxel size of 15 μ m. We segmented trabecular bone from the cortex using a semi-automated contouring algorithm in the axial plane. We selected LV₃ for spine, and the ROI included the middle 1/3 of the vertebral bodies' equivalent to 2.1 mm. For cortical analysis, we chose a region of 0.75 mm along the femoral midshaft.

Mechanical testing We prepared 6 specimens/group for strength testing of the fourth lumbar vertebral bodies using a low-speed diamond saw to remove posterior elements and endplates. We performed destructive four-point bend tests on 9 rats/group of the right femurs with a span between the two lower supports set at 14 mm, and the span between the two upper loads set at 7 mm. We conducted testing at a displacement rate of 5 mm/min. Structural parameters, maximum load, stiffness, and energy absorption data were generated from the load-displacement curve for each specimen (Instron 4465/5500; Instron, Norwood, MA).

Raman spectroscopy analysis. We assessed cortical bone mineralization by calculating the intensity of several vibrational bonds, which are highly specific to chemical content, using the

Raman scattering effect. We chose four femurs from each group based on disparities in femoral bone volume. We acquired spectra from the bone surface on the anterior side of the proximal, distal, and mid-diaphysis regions with an exposure time of 300 s per region. The locally constructed Raman spectroscopy system used to acquire these spectra has been described previously (Maher et al. 2011). This instrument has a large depth of focus (the illumination numerical aperture is 0.05). Therefore, each measurement probed a large, macroscopic volume of cortical bone. We characterized differences in mineral and protein content between the rat femurs by metrics related to bone biochemistry including the mineral-to-matrix ratio (MTMR; $\text{PO}_4^{3-} / \text{CH}_2$ peak area ratio). It should be noted that the effects of polarization were not explored in this study since the illumination was not highly polarized.

Bone histomorphometry and immunohistochemistry. We stripped proximal tibia of soft tissues and fixed in formalin for 4 days, decalcified, paraffin embedded and sectioned as described previously (Carmouche et al. 2005). We calculated static parameters and expressed them according to published methods using Osteomeasure bone analysis software (Osteometrics, Decatur, GA). ROI for tibial trabecular bone was an area (1.23 mm^2) below the growth plate within the metaphysis. For intramedullary fat analysis, we counted the number of fat vacuoles in bone marrow, which appear optically empty in sections. For immunohistochemistry, we deparaffinized sections from 3 rats/group in xylene and antigen retrieval performed in 10 mM citrate buffer, pH 6.0, for 1 h at 80°C for β -catenin (1:30, Cell Signaling Technologies, Danvers, MA) and 30 m for both sclerostin (1:50, R&D Systems, Minn., MN, USA) and Runx2 (1:100, MLB International, Woburn, MA). We incubated sections overnight at 4°C with primary antibodies. We washed sections in PBS and incubated them in appropriate secondary antibodies (1:200; Vector Laboratories, Burlingame, CA) for 30 minutes, followed by horseradish peroxidase

streptavidin (1:750; Zymed, San Francisco, CA) for 30 min and developed with AEC chromogen for 10 minutes.

Cellular assays. Osteoblastogenesis: We isolated primary rat calvarial osteoblasts from 3-day old neonatal pups as described previously (Ryan et al. 2007). We cultured the cells in osteogenic alpha-MEM in the presence of increased dosing of Pb, 0.8-5.0 μ M. After 18 days in culture, we washed the cells twice with normal saline and fixed with 10% formalin and stained with 0.1% alizarin red (95% ETOH) for 20 minutes.

Adipogenesis: We pretreated C3H10t1/2 cells for 5 days with Pb during the proliferative phase and early confluence in high glucose DMEM with 10%. Two days post-confluence, we treated the cells with hormone cocktail of methylisobutylxanthine, dexamethasone, and insulin in Pb-free complete DMEM in accordance with standard adipogenesis protocols in this cell line (Cho and Jefcoate 2004). We stained lipid droplets 5 days later with Oil-Red-O (2.1mg/ml [4 isopropanol:3 water]) for 1 hour at room temperature. We achieved quantification of stained area by dissolving stain in 4% IGEPAL (v/v isopropanol) and measuring absorption at 490 nm.

We isolated total RNA and protein on day 10 for osteoblasts and day 5 for adipocytes with concurrent Pb treatment, 0.8-5.0 μ M for RNA and 1.0-5.0 μ M for protein. RNeasy Plus Mini Kit (Qiagen) was used for RNA isolation according to the manufacturer's protocols. We performed rt-PCR reactions as described earlier. We conducted protein analysis as described previously (Ryan et al. 2007) using polyclonal rabbit Runx-2, collagen 1, β -actin (Abcam, Cambridge, MA), PPAR γ (peroxisome proliferator-activated receptor- γ), C/EBP β , C/EBP α (Santa Cruz Biotechnology, Santa Cruz, CA), monoclonal mouse β -catenin (Santa Cruz), or polyclonal goat sclerostin and DKK-1 (R&D Systems).

Statistical Analysis. Results are expressed as the sample mean \pm standard error. We used an unpaired Student's t-test to determine statistical differences with $P \leq 0.05$, and one-way ANOVA followed by the Tukey multiple comparison test to determine dose-dependent effects. In addition, we used univariate regression to predict the energy to failure of each femur based upon Raman MTMR. We used a leave-one-out cross-validation approach and prediction accuracy was quantified by calculating the squared sample correlation coefficient (r^2).

Results

Effect of Pb on tissue exposure and BMD in aged rats. During the course of treatment, we monitored Pb exposure levels in the rats (Cory-Slechta et al. 2010). At 18 months old, background BLL in the unexposed rats was 0.19 $\mu\text{g}/\text{dL}$ as compared to 9.16 $\mu\text{g}/\text{dL}$ in the Pb exposed animals. The Pb content in tibia was 30.99 $\mu\text{g Pb}/\text{g}$ dry bone, versus 0.17 $\mu\text{g}/\text{g}$ in control rats. We took x-rays on whole limbs and lumbar spinal columns *ex vivo* (Figure 1A-D). Radiographs of Pb-exposed animals show a decrease in trabecular bone in both the long bones and spine as visualized by increased radiolucency in these regions. *Ex vivo* DXA analysis demonstrated that compared to control animals, Pb-exposed rats had significantly decreased areal BMD at the femur-tibia region (-4.7%, $*p = 0.04$) and a trend toward decreased BMD at lumbar vertebrae 1–5 (-4.9%, $p = 0.09$) (Figure 1E,F).

We performed micro-CT analysis of trabecular bone at the third lumbar (LV3) vertebrae (Figure 2A). Quantitative measures of trabecular bone quality showed a significant decrease in BV/TV (-27%), Tb N (-23%), Conn D (-34%), and increase in Tb Sp (+30%) in Pb-treated rats over controls. Similarly, the metaphyseal region of the distal femur demonstrated a reduction of trabecular bone volume caused by Pb exposure. Quantitative analysis of the trabecular bone

showed that Pb-treated rats had significantly depressed bone properties (BV/TV -33%, Tb.N -48%, Conn D -61%, Tb.Sp +100%) compared with controls (Figure 2B). Micro-CT analysis of trabecular bone in the proximal tibia showed an analogous decrease in trabecular bone volume (BV/TV, -32%) for Pb-treated rats compared with control animals (Figure 2C). Trabecular thickness was unchanged in all bones with Pb exposure; therefore, the decreases in bone volume in Pb animals could be attributed to the significant reduction in Tb.N (-44%). This corresponded to an increase in Tb.Sp (+83%) and a decrease in Conn D (-61%). All together these data indicate that low-level Pb contributes to a systemic decrease in skeletal mass. Micro-CT analysis of the femoral midshaft showed that Pb-treated rats had significantly decreased cortical bone area (-7%) and cortical thickness (-8%) compared with controls (Figure 3A).

Biomechanical strength is altered in Pb treatment at lumbar vertebrae and femoral midshaft.

To assess bone strength, we conducted compression testing of the third lumbar vertebrae and measured maximum load, stiffness, and energy to failure. Vertebral bone strength in Pb-treated rats was reduced as significant decreases were observed in maximum load (-35%) and maximum stiffness (-28%) compared with controls (see Supplemental Material, Table S2). The decreased femoral bone mass and thickness observed in micro-CT of Pb-treated rats translated into lower bone strength as demonstrated by significant decreases in both maximum load (-23%), energy to failure (-31%), and force at yield (-26%) for Pb-treated animals compared with controls

Effect of Pb on biochemical composition of bone as measured by Raman spectroscopy. We

acquired the average Raman spectra from rat femurs and overlaid them in Figure 3B. Major Raman peaks associated with mineral (PO_4^{3-} and CO_3^{2-}) and protein matrix (amide III, CH_2 , and amide I) content are labeled. The intensities of several peaks (e.g. PO_4^{3-} and CO_3^{2-}) are quantified by the Raman parameters (see Supplemental Material, Table S2). The divergence in

each of these parameters was statistically significant; the MTMR and crystallinity were smaller and the CTPR and collagen maturity were greater in the rats exposed to Pb. Scatter plots of energy to failure as predicted by univariate regression against the Raman spectroscopy-derived MTMR, DXA areal BMD, micro-CT Cort Th is presented in Figure 3C. The MTMR-based predictions were more highly correlated ($r^2 = 0.81$) with the energy to failure than predictions based upon individual micro-CT parameter ($r^2 < 0.6$) or areal BMD ($r^2 = 0.03$).

Histomorphometric analysis of proximal tibia. To further determine the effect of Pb on bone, we calculated histomorphometric parameters relating to bone formation and bone resorption in trabecular bone of the proximal tibia. We observed a consistent decrease in trabecular bone volume (BV/TV, -56%) for Pb-treated rats compared with control animals (Figure 4A). There was also significantly reduced area of cartilage bars present in the Pb-treated animals (-70%). Furthermore, osteoblast numbers (#Ob/Tb Ar) were significantly reduced compared with controls. Histology-based bone resorption parameters (#Oc/Tb Ar, Oc.S/BS) remained approximately the same in Pb exposed animals compared with controls. There was no apparent change in the amount or structure of woven bone between the two groups (see Supplemental Figure S1C). We observed no change in cell viability in the osteocytes in trabecular and cortical bone of Pb rats compared to controls using TUNEL staining (see Supplemental Figure S1A,B). We determined bone marrow composition by comparing the adipocyte content within the trabecular region. Adipocyte volume (+112%) and number (+52%) were increased, where size was not significantly changed in Pb exposed rats (Figure 4B).

Analysis of Pb on Wnt signaling. In attempt to uncover the molecular signaling changes fundamental to the apparent decrease in bone formation properties and increase in bone marrow adiposity, we measured the expression of several important proteins essential for these bone

processes. Sclerostin is robustly expressed in mature osteoblasts and osteocytes and is present in the bone matrix (Figure 5A,B). We observed an increase in sclerostin staining around the epiphyseal region in trabecular bone osteocytes (green arrows), and increased deposition in the bone matrix of Pb exposed rats (blue arrows). Expression of β -catenin is concentrated in the osteoprogenitor cells that line the trabecular regions (Figure 5C,D). Staining for β -catenin showed a decrease in frequency and intensity of expression in the stromal lining cells (black arrows) in Pb exposures compared to control rats. Runx2, a key transcriptional regulator of bone formation, is abundantly expressed in osteoblasts and osteocytes; however, the number of positive cells as well as the staining intensity was dramatically decreased in Pb-exposed animals (Figure 5E,F).

Real-time PCR analysis of mRNA levels of the bone forming gene *osteocalcin* (-68%), the Wnt signaling molecule *β -catenin* (-26%) and the osteoblast differentiation transcription factor *Runx2* (-57%) were decreased with Pb exposure (Figure 5G), which is consistent with histological findings. At the same time, mRNA levels of pro-adipogenic genes *PPAR- γ* (+253%) and *aP2* (+389%) were elevated in Pb exposed animals (Figure 5H).

Pb induces adipogenesis and inhibits bone nodule formation. We set out to determine the effect of Pb on two aspects of bone homeostasis: mesenchymal cell differentiation to adipocytes and osteoblasts. Alizarin Red staining revealed that Pb-treated primary cultures produced significantly less mineralized nodules in a dose dependent fashion from 1 μ M - 5 μ M (Figure 6A,B). This indicates a direct inhibitory effect of Pb on osteoblast differentiation *in vitro*. Consistent with this, we observed a reduction in expression of the osteoblastic genes *type 1 collagen*, *ALP*, and *OC* (Figure 6C). Pro-osteoblastic transcription factors *β -catenin*, *Runx-2*,

and *osterix* were also dose dependently decreased by Pb, and we observed an elevation in sclerostin protein follow Pb exposure.

Alternatively, pretreatment of Pb enhanced the adipogenic potential of mouse embryonic fibroblasts *in vitro*. Oil-Red-O staining revealed that there was a 4-fold increase in lipid droplets as a result of Pb exposure at 2 μ M (Figure 6A,B). Enhanced adipogenesis was supported by the increase in expression of pro-adipogenic factors *PPAR- γ* , *C/EBP* isoforms, *aP2*, and *cdf* (Figure 6D). This was accompanied by an elevation of DKK-1.

Discussion

Our results indicate that long-term Pb exposure evokes significant skeletal changes consistent with a low bone mass phenotype resembling osteoporosis at continuous blood levels below 10 μ g/dL in adult rats. We designed the exposure paradigm utilized in this study to represent one that is relevant to current environmental exposure in the United States today. It is the lowest cumulative exposure studied to evaluate the effect of Pb on bone quality. Bone densitometry measurements demonstrated a lower bone mass and corresponding decreased resistance to biomechanical forces, suggesting a higher susceptibility to fracture. These findings: deterioration of trabecular architecture, decreased bone mass, and decreased cortical thickness, have been implicated in reduced bone strength and increased fracture incidence in humans (Barth et al. 1992; Wachter et al. 2002). Additionally, the observed biochemical differences in mineral and protein matrix content, as measured by Raman spectroscopy, suggest that long term Pb exposure causes specific chemical changes in bone, which indicates some degree of altered cell function of osteocytes within the cortical bone sites. These findings are in agreement with a

previous report demonstrating reduction in mineral crystal size and decreased MTMR in mouse bones exposed to Pb (Monir et al, 2010).

Decreased BMD and an increased fracture risk are hallmarks of osteoporosis; thus, our observed association of decreased BMD and bone strength with Pb exposure raises concern for Pb as a risk factor for osteoporosis in aged individuals. Currently there is limited data on human bone outcomes and Pb. However, Khalil et al. (2008) published that elevated BLLs are associated with an increased risk of falls and nonspine fractures, further validating this concern. Moreover, osteoporotic patients have a decreased capacity to heal fractures. Animal studies also suggest that fracture healing is suppressed by Pb exposure (Carmouche et al. 2005). BMD obtained from DXA is the current gold standard used to predict risk; however we hypothesize that DXA predictions of fracture risk due to Pb exposure might underestimate actual fracture risk. The results of this study suggest that Raman spectra of bone, if obtained transcutaneously, may be capable of contributing to the prediction of fracture risk in patients exposed to Pb. Although these preliminary predictive results are compelling, they are based only upon simple univariate regressions and more complex multivariate prediction models could potentially provide more accurate predictions (Maher et al. 2011).

At the sub toxic Pb concentrations presented in this study, there is an impact of Pb on bone homeostasis that results in decreased bone mass. Specifically, bone mass decreases were accompanied by a reduction in osteoblast number suggesting a depression of bone formation, as opposed to no significant change in osteoclast frequency or bone resorption. Additionally, there was an increase in the number of adipocytes suggesting a possible increase in adipogenesis. The increased expression of *PPAR γ* further supports this claim. Despite decades of knowledge of the detrimental effects of Pb on bone health, remarkably little is known of the mechanisms by which

they occur. Wnt signaling is a very active anabolic pathway in bone and was therefore hypothesized as a target for Pb toxicity. To this end we discovered a strong up-regulation of the Wnt inhibitory factor, sclerostin, and analogous reduction of β -catenin. Correspondingly, Runx-2 levels were depressed in Pb-treated rats. These findings support the hypothesis that Pb inhibits Wnt signaling leading to reduced osteoblast activity. Moreover, they substantiate the *in vitro* acceleration of adipocyte formation and inhibition of bone nodule formation following Pb treatment. Depression of Wnt signaling has also been demonstrated to decrease adipogenesis by preventing the activation of pro-adipogenic factors that are required for progression of adipocyte formation (Li et al. 2007; Ross et al. 2000). This suggests that Pb inhibition of Wnt signaling can act as a molecular trigger to increase adipocyte frequency. Other environmental stressors, such as ethanol, have also been demonstrated to influence mesenchymal commitment via inhibition of Wnt signaling (Chen et al. 2010). Currently there are human clinical trials using sclerostin and DKK antibodies to treat diseases of low bone mass signifying the pathogenic nature of these molecules (Fulciniti et al. 2009; Padhi et al. 2011). Thus, we believe that the observed depression of Wnt/ β -catenin both *in vivo* and *in vitro* through sclerostin is an important mechanism for Pb toxicity in the skeleton. In all, our findings support the hypothesis that Pb can influence mesenchymal cell differentiation into osteoblasts or adipocytes through modulation of Wnt signaling.

The Pb induced osteoporotic-like phenotype described here is remarkably similar and parallels symptoms and sequelae of human of osteoporosis. Specifically, the human condition of osteoporosis is often characterized by decreased number of bone forming cells causing depression of formation, unfilled resorptive surfaces, and a conversion of bone marrow to increased adiposity (Gimble et al. 2006; Nuttall and Gimble 2004; Syed et al. 2008; Verma et al.

2002). All of these observations were present in our Pb-treated rat population. These two converging pathologies, depressed bone formation and increased adipogenesis, helps further our understanding of how Pb is a risk factor for osteoporosis by unbalancing bone homeostasis with reduction of Wnt signaling. These findings indicate that Pb has a detrimental impact in bone at levels previously thought safe. This study in conjunction with others indicating low-level Pb effects need to be considered when evaluating Pb policy concerning adverse effect levels.

References

- Bagchi D, Preuss HG. 2005. Effects of acute and chronic oval exposure of lead on blood pressure and bone mineral density in rats. *J Inorg Biochem* 99(5):1155-1164.
- Barth RW, Williams JL, Kaplan FS. 1992. Osteon morphometry in females with femoral neck fractures. *Clin Orthop Relat Res* 283:178–186.
- Campbell JR, Auinger P. 2007. The association between blood lead levels and osteoporosis among adults--results from the third national health and nutrition examination survey (NHANES III). *Environ Health Perspect* 115(7):1018-1022.
- Carmouche JJ, Puzas JE, Zhang X, Tiyyapanaputi P, Cory-Slechta DA, Gelein R, et al. 2005. Lead exposure inhibits fracture healing and is associated with increased chondrogenesis, delay in cartilage mineralization, and a decrease in osteoprogenitor frequency. *Environ Health Perspect* 113(6):749-755.
- Centers for Disease Control (U.S.). 1991. Preventing lead poisoning in young children: a statement by the centers for disease control. Atlanta, GA: The Centers vi, 108.
- Chen JR, Lazarenko OP, Shankar K, Blackburn ML, Badger TM, Ronis MJ. 2010. A role for ethanol-induced oxidative stress in controlling lineage commitment of mesenchymal stromal cells through inhibition of Wnt/beta-catenin signaling. *J Bone Miner Res* 25(5):1117-1127.
- Cho YC, Jefcoate CR. 2004. PPARgamma1 synthesis and adipogenesis in C3H10T1/2 cells depends on S-phase progression, but does not require mitotic clonal expansion. *J Cell Biochem* 91(2):336–353.
- Cory-Slechta DA, Stern S, Weston D, Allen JL, Lui S. 2010. Enhanced learning deficits in female rats following lifetime pb exposure combined with prenatal stress. *Toxicol Sci* 117(2):427-438.
- Dowd TL, Rosen JF, Mints L, Gundberg CM. 2001. The effect of Pb(2+) on the structure and hydroxyapatite binding properties of osteocalcin. *Biochim Biophys Acta* 1535:153-163.
- Escribano A, Revilla M, Hernandez ER, Seco C, Gonzalez-Riola J, et al. 1997. Effect of lead on bone development and bone mass: a morphometric, densitometric, and histomorphometric study in growing rats. *Calcif Tissue Int* 60(2):200-203.

- Fulciniti M, Tassone P, Hideshima T, Vallet S, Nanjappa P, Ettenberg SA, et al. 2009. Anti-DKK1 mAb (BHQ880) as a potential therapeutic agent for multiple myeloma. *Blood* 114(2):371-379.
- Goyer RA. 1993. Lead Toxicity: Current Concerns. *Environ Health Perspect* 100:177-187.
- Gruber HE, Gonick HC, Khalil-Manesh F, Sanchez TV, Motsinger S, et al. 1997. Osteopenia induced by long-term, low- and high-level exposure of the adult rat to lead. *Miner Electrolyte Metab* 23(2):65-73.
- Gimble JM, Zvonic S, Floyd ZE, Kassem M, Nuttall ME. 2006. Playing with bone and fat. *J Cell Biochem* 98(2):251-266.
- Guo R, Yamashita M, Zhang Q, Zhou Q, Chen D, Reynolds DG, et al. 2008. Ubiquitin ligase Smurf1 mediates tumor necrosis factor-induced systemic bone loss by promoting proteasomal degradation of bone morphogenetic signaling protein. *J Biol Chem* 283(34):23084-23092.
- Johnson ML, Harnish K, Nusse R, Van Hul W. 2004. LRP5 and Wnt signaling: a union made for bone. *J Bone Miner Res* 19(11):1749-1757.
- Johnson ML, Gong G, Kimberling W, Recker SM, Kimmel DB, Recker RB. 1997. Linkage of a gene causing high bone mass to human chromosome 11 (11q12-13). *Am J Hum Genet* 60(6):1326-1332.
- Khalil N, Cauley JA, Wilson JW, Talbott EO, Morrow L, Hochber MC, et al. 2008. Relationship of blood lead levels to incident nonspine fractures and falls in older women: the study of osteoporotic fractures. *J Bone Miner Res* 23(9):1217-1225.
- Klein RF, Wren KM. 1993. Regulation of osteoblastic gene expression by lead. *Endocrinology* 132:2531-2537.
- Li FQ, Singh AM, Mofunanya A, Love D, Terada N, Moon RT, et al. 2007. Chibby promotes adipocyte differentiation through inhibition of beta-catenin signaling. *Mol Cell Biol* 27(12):4347-4354.
- Li X, Zhang Y, Kang J, Liu W, Liu P, Zhang J, et al. 2005. Sclerostin binds to LRP5/6 and antagonizes canonical Wnt signaling. *J Biol Chem* 280(20):19883-19887.
- Li X, Ominsky MS, Warmington KS, Morony S, Gong J, Cao J, et al. 2009. Sclerostin antibody treatment increases bone formation, bone mass, and bone strength in a rat model of postmenopausal osteoporosis. *J Bone Miner Res* 24(4):578-588.

- Li X, Ominsky MS, Niu QT, Sun N, Daugherty B, D'Agostin D, et al. 2008. Targeted deletion of the sclerostin gene in mice results in increased bone formation and bone strength. *J Bone Miner Res* 23(6):860-869.
- Mahaffey KR, Annett JL, Roberts J, Murphy RS. 1982. National estimates of blood lead levels: United States, 1976-1980: association with selected demographic and socioeconomic factors. *N Engl J Med* 307:573-579.
- Maher JR, Takahata M, Awad HA, Berger AJ. 2011. Raman spectroscopy detects deterioration in biomechanical properties of bone in a glucocorticoid-treated mouse model of rheumatoid arthritis. *J Biomed Opt* 16(8):087012.
- Monir AU, Gundberg CM, Yagerman SE, van der Meulen MCH, Budell W, Bosky AL, Dowd TL. 2010. The effect of lead on bone mineral properties from female adult c57/bl6 mice. *Bone* 47(5):888-894.
- Nash D, Magder LS, Sherwin R, Rubin FJ, Silbergeld EK. 2004. Bone density-related predictors of blood lead level among peri- and postmenopausal women in the United States: The Third National Health and Nutrition Examination Survey, 1988-1994. *Am J Epidemiol* 160(9):901-911.
- Nuttall ME, Gimble JM. 2004. Controlling the balance between osteoblastogenesis and adipogenesis and the consequent therapeutic implications. *Curr Opin Pharmacol* 4(3):290-294.
- Parsons PJ. 1993. A rapid Zeeman graphite furnace atomic absorption spectrometric method for the determination of lead in blood. *Spectrochim Acta* 48B:925-939.
- Padhi D, Jang G, Stouch B, Fang L, Posvar E. 2011. Single-dose, placebo-controlled, randomized study of AMG 785, a sclerostin monoclonal antibody. *J Bone Miner Res* 26(1):19-26.
- Puzas JE, Campbell JR, O'Keefe RJ, Rosier RN. 2004. Lead toxicity in the skeleton and its role in osteoporosis. *Nutrition and Bone Health Ch* 22:363-376.
- Robinson JA, Chatterjee-Kishore M, Yaworsky PJ, Cullen DM, Zhao W, Li C, et al. 2006. Wnt/beta-catenin signaling is a normal physiological response to mechanical loading in bone. *J Biol Chem* 281(42):31720-31728.
- Ross SE, Hemati N, Longo KA, Bennett CN, Lucas PC, Erickson RL, et al. 2000. Inhibition of adipogenesis by Wnt signaling. *Science* 289(5481):950-953.

- Ryan EP, Holz JD, Mulcahey M, Sheu TJ, Gasiewicz, TA, Puzas JE. 2007. Environmental Toxicants May Modulate Osteoblast Differentiation by a Mechanism Involving the Aryl Hydrocarbon Receptor. *J Bone Miner Res* 22(10):1571–1580.
- Sauk JJ, Smith T, Silbergeld EK, Fowler BA, Somerman MJ. 1992. Lead inhibits secretion of osteonectin/SPARC without significantly altering collagen or Hsp47 production in osteoblast-like ROS 17/2.8. *Toxicol Appl Pharmacol* 116(2):240-247.
- Shahnazari M, Yao W, Corr M, Lane NE. 2008. Targeting the Wnt signaling pathway to augment bone formation. *Curr Osteoporos Rep* 6(4):142-148.
- Syed FA, Oursler MJ, Hefferanm TE, Peterson JM, Riggs BL, Khosla S. 2008. Effects of estrogen therapy on bone marrow adipocytes in postmenopausal osteoporotic women. *Osteoporos Int* 19(9):1323-1330.
- van Bezooijen RL, ten Dijke P, Papapoulos SE, Lowik CW. 2005. SOST/sclerostin, an osteocyte-derived negative regulator of bone formation. *Cytokine Growth Factor Rev* 16(3):319-327.
- Verma S, Rajaratnam JH, Denton J, Hoyland JA, Byers RJ. 2002. Adipocytic proportion of bone marrow is inversely related to bone formation in osteoporosis. *J Clin Pathol* 55(9):693-698.
- Wachter NJ, Krischak GD, Mentzel M, Sarkar MR, Ebinger T, Kinzl L, et al. 2002. Correlation of bone mineral density with strength and microstructural parameters of cortical bone in vitro. *Bone* 31(1):90–95.

Figure Legends

Figure 1

Pb exposure decreased bone mineral density in rat long bones and lumbar vertebrae. Rats were continuously exposed to 50 ppm Pb in drinking water. Representative radiographic images taken ex vivo from randomly selected rats in each group are displayed. Arrows indicate the radiolucency that is more prominent in the trabecular region of Pb exposed rats (**B, D**), which is absent in the unexposed animals (**A, C**). DXA scans detected lower areal BMD in both leg and spine of the Pb exposed rats (**E, F**). Scale Bar: 2.5 mm. Data represent mean \pm SEM for 9 rats/group, $*p < 0.05$.

Figure 2

Exposure to 50 ppm Pb results in a systemic decrease in trabecular bone volume. We analyzed trabecular (Tb) bone properties in the following regions of interest: the third lumbar vertebrae (**A**), the distal femur (**B**) and proximal tibia (**C**). Representative images are transverse section from control and Pb-exposed groups, and selected based on the median trabecular bone volume (BV/TV). Graphs show significant changes in bone volume, trabecular number, trabecular spacing, and connective density. Scale Bar: 2.5 mm (**A**), 1 mm (**B, C**). Data represent mean \pm SEM for 9 rats/group, $*p < 0.05$.

Figure 3

Pb treatment alters bone properties at the femoral midshaft. **(A)** Micro-CT analysis of rat femurs generated data for cortical thickness and bone area. A representative cross-sectional image is present from both groups. **(B)** Average Raman spectrum acquired from each femur, control in blue and Pb in red. The difference in phosphate chemical peaks is expanded. **(C)** Scatter plots of the MTMR, areal BMD, and Cort Th-based predictions of the energy-to-failure for each femur versus its measured value from Supplemental Table S3. Scale Bar: 1 mm. Data represent mean \pm SEM for 9 rats/group for micro-CT and 4 rats/group for Raman, $*p < 0.05$.

Figure 4

Changes in bone and adipogenic histomorphometric parameters in Pb exposed rats. **(A)** We evaluated trabecular bone in the metaphyseal region of proximal tibia in control and Pb-treated rats for the following bone properties: BV/TV, bone volume over total volume; Cart Ar/Tb Ar, cartilage area over trabecular area; # Ob/Tb.Ar, osteoblast number over trabecular area; # Oc/Tb.Ar, osteoclast number over trabecular area; Oc.S/BS, osteoclast surface over bone surface. **(B)** Magnified images from black boxes showing fatty bone marrow changes in rat tibia. Green arrows highlight areas of unfilled tunneling and resorption space in Pb exposures. Black arrows indicate the cartilage bars in trabecular bone. Data represent mean \pm SEM for 4 rats/group, $*p < 0.05$. Scale bar: **(A)** 100 μm , **(B)** 500 μm .

Figure 5

Pb decreases osteogenesis by up-regulation of sclerostin and corresponding suppression of Wnt signaling and osteoblastic genes, while also increasing adipogenesis. (**A-F**) Represented immunohistochemistry staining in proximal tibia for protein expression using antibodies against sclerostin, β -catenin, and RunX2. Green arrows point out osteocytes, black arrows are stromal cells, and blue arrows are highlighting bone matrix. Scale bar: 100 μ m. (**G**) *Osteocalcin*, β -*catenin*, *RUNX-2*, (**H**) *PPAR- γ* , and *aP2* gene expression from isolated total RNA in rat tibias (n=4) using RT-PCR. Data represent mean \pm SEM, * $p < 0.05$, ** $p < 0.005$.

Figure 6

Pb increases the adipogenic potential of mesenchymal cells while suppressing osteoblast differentiation by corresponding reduction of Wnt signaling. (**A**) Pb dose-dependently increases the adipogenic potential of progenitor cells treated with an adipogenic cocktail and stained with Oil-red-O, while also inhibiting mineralization of primary osteoblasts as seen with alizarin red stain. Quantification of stains is in panel **B**. (**C**) Expression profile of osteoblastic genes and protein levels following 10 days Pb exposure. (**D**) Expression profile of adipogenic genes and protein levels following 5 days Pb exposure. Data represent mean \pm SEM for 3 trials, * $p < 0.05$, ** $p < 0.005$.

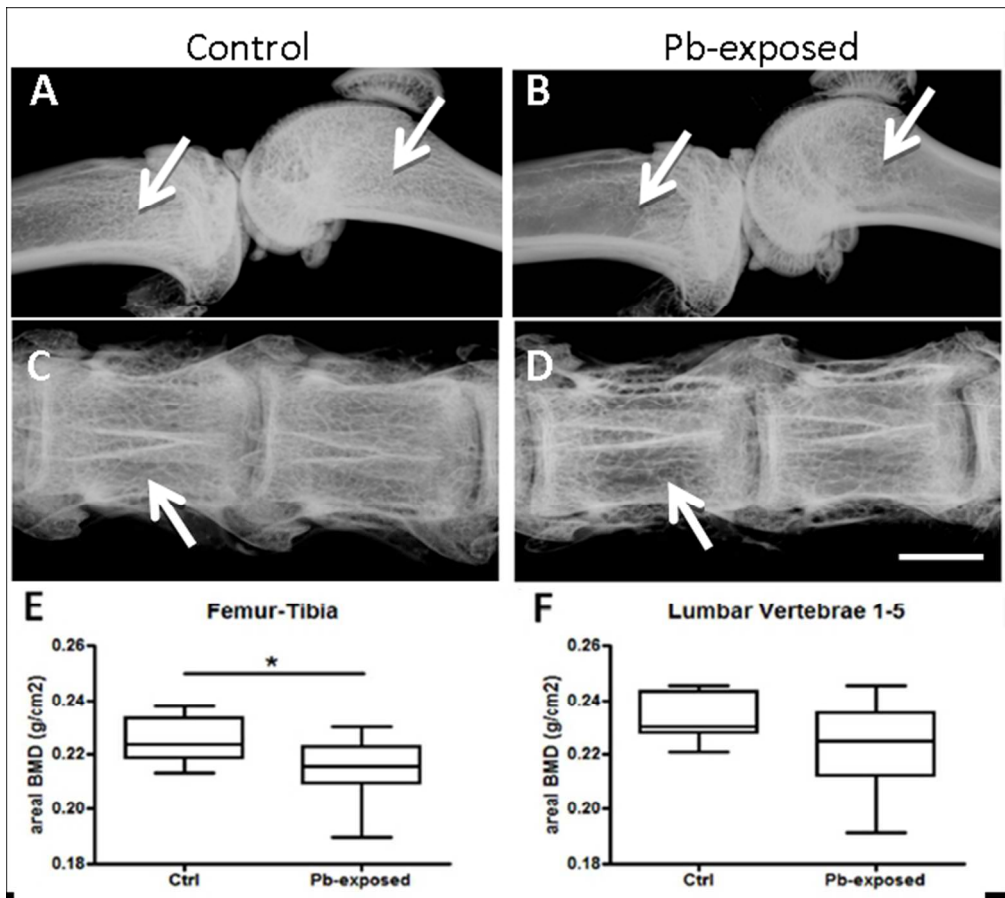


Figure 1
118x106mm (150 x 150 DPI)

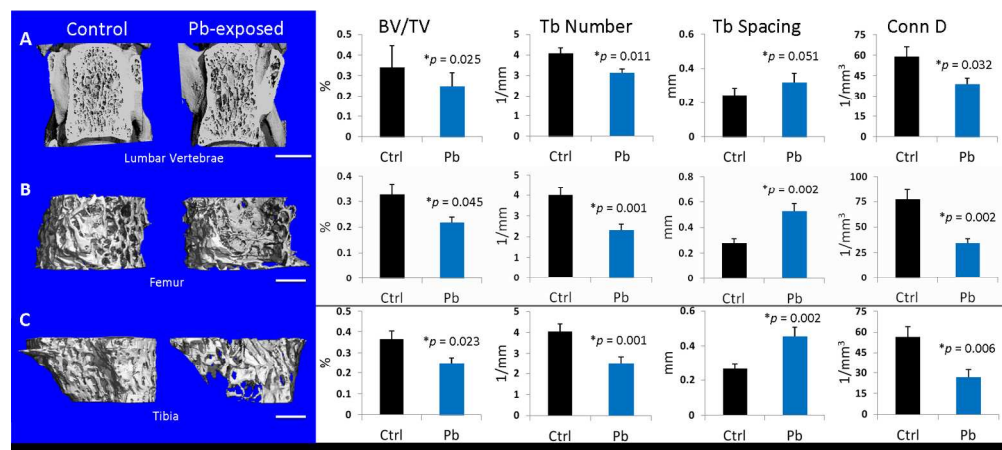


Figure 2
315x140mm (150 x 150 DPI)

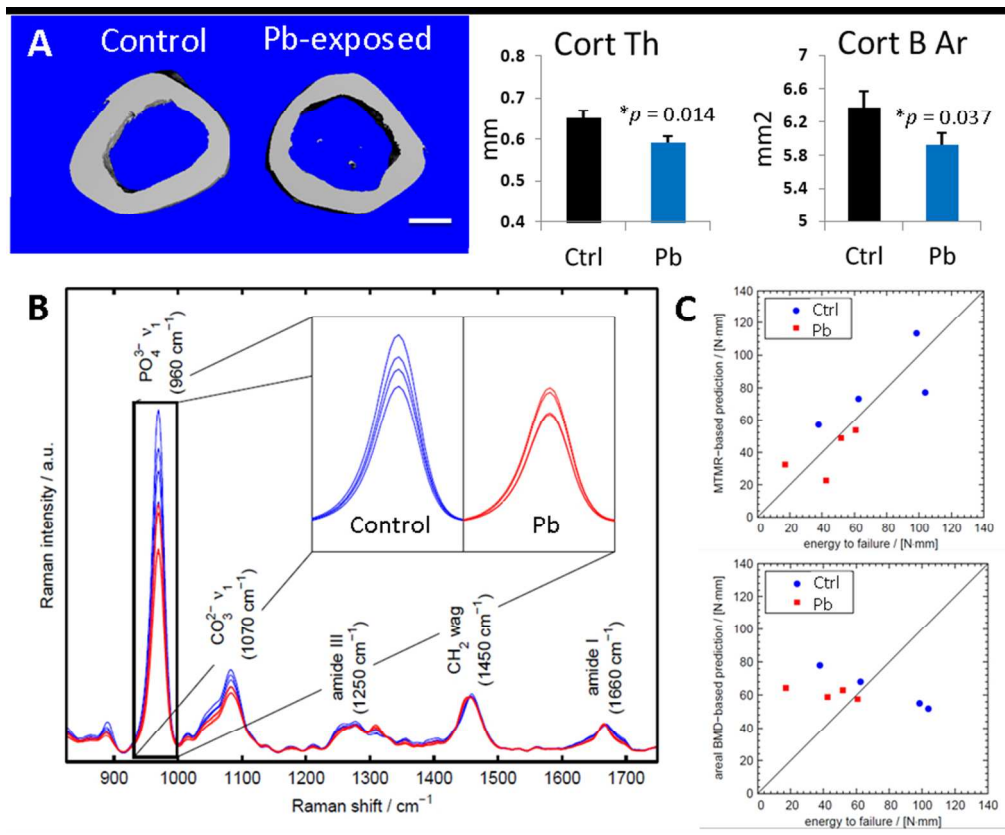


Figure 3
156x129mm (150 x 150 DPI)

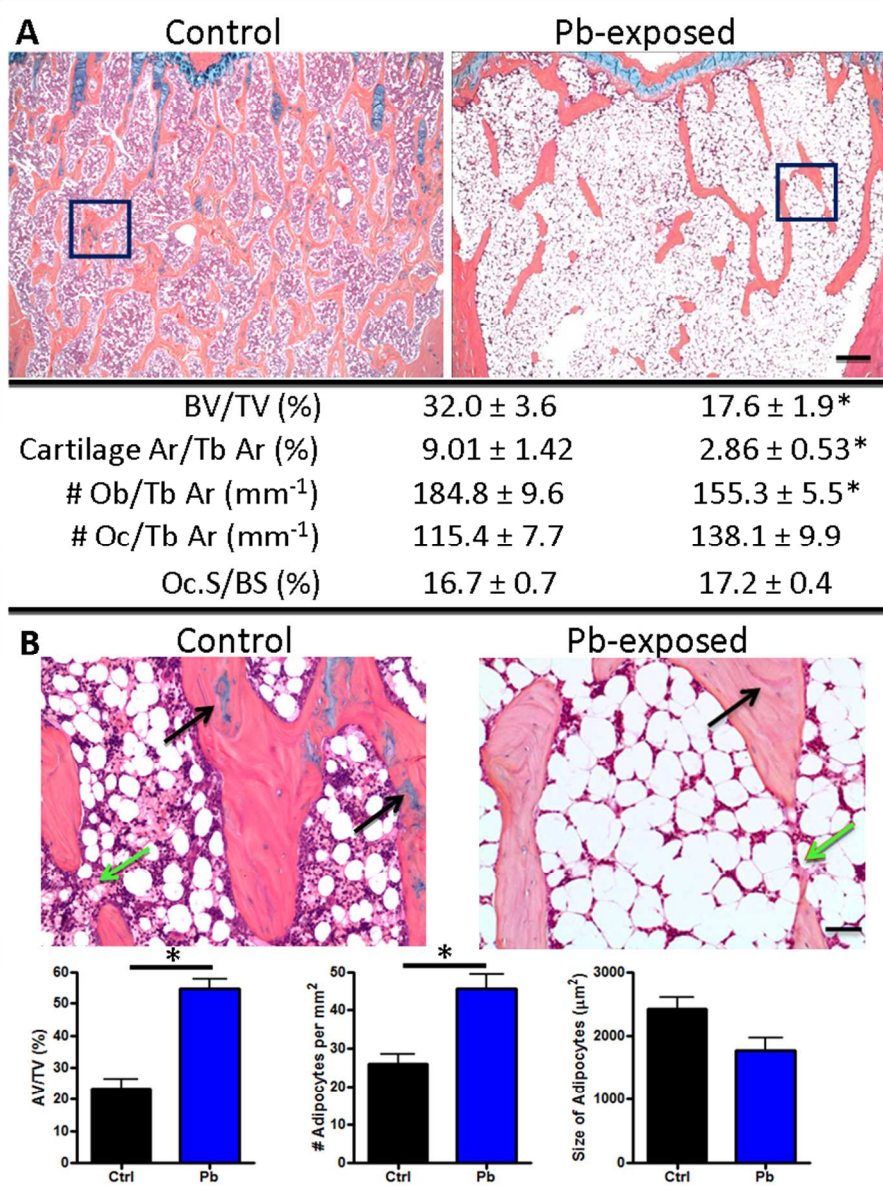


Figure 4
150x198mm (150 x 150 DPI)

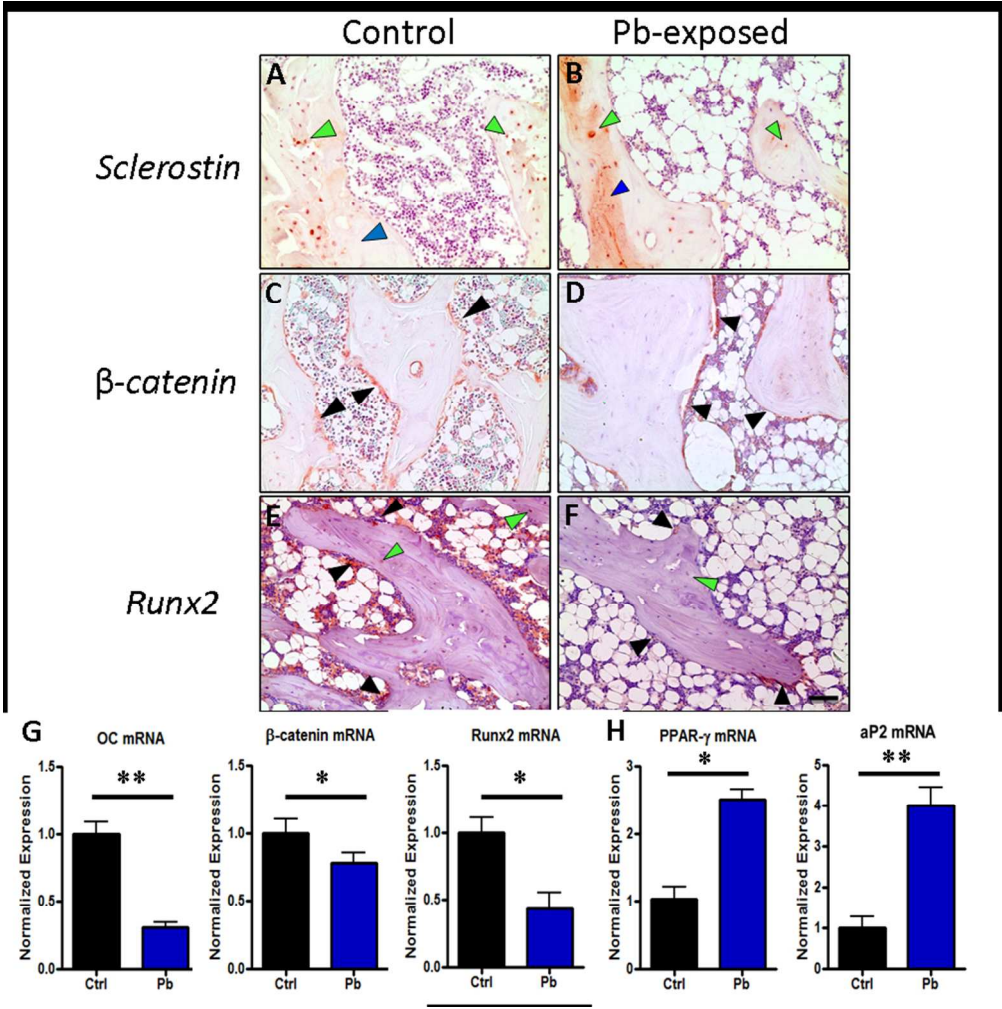


Figure 5
170x171mm (150 x 150 DPI)

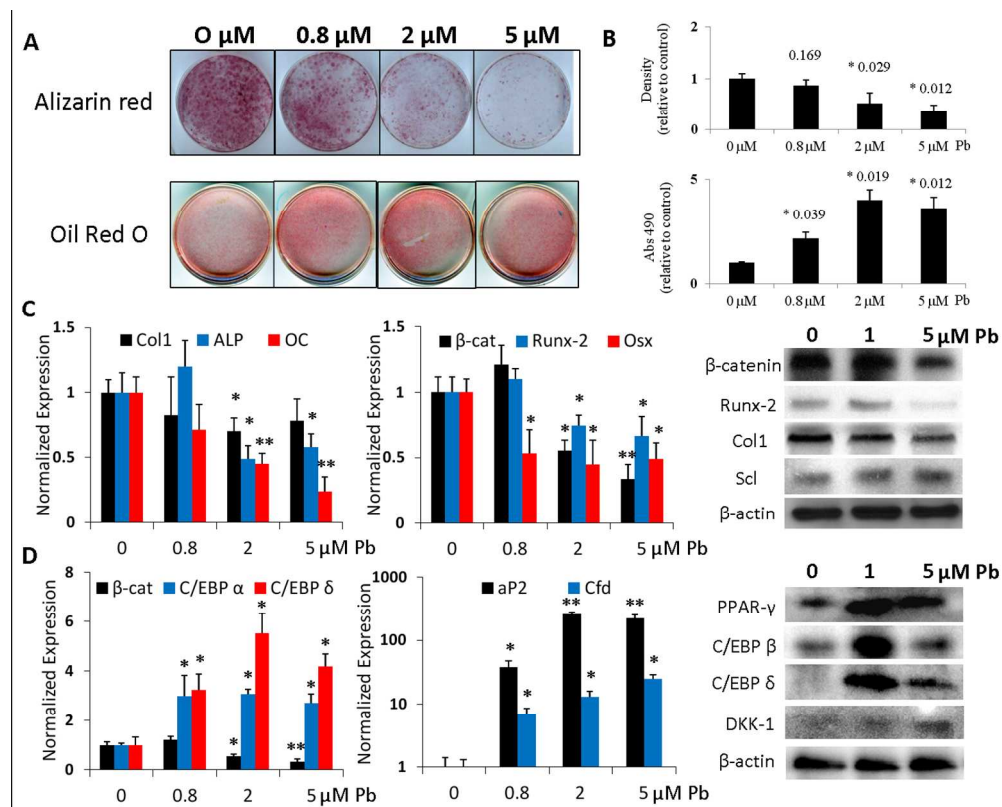


Figure 6
247x198mm (150 x 150 DPI)